Applied Physics A (2022) 128:889
https://doi.org/10.1007/s00339-022-05992-1

Applied Physics A
Materials Science & Processing

S.I. : COLA 2021/2022

Investigation of the effects of pulse width modulation on the laser sintering of LATP for all-solid-state batteries

H. Wehbe[1] · L. O. Schmidt[1] · M. W. Kandula[1] · K. Dilger[1]

Received: 28 April 2022 / Accepted: 23 August 2022 / Published online: 16 September 2022

Abstract
Inorganic solid electrolytes are the most important component for realizing all-solid-state batteries with lithium metal anodes and enable safe battery cells with high energy densities. Their synthesis and processing are the subject of current research, especially the NASICON-type $Li_{1+x}AlxTi_{2-x}(PO_4)_3$ (LATP). Herein, the ability of sintering with electro-magnetic irradiation is investigated and correlated with different properties of prepared LATP pellets. First of all, an infrared camera records the temperature of the surface during the treatment. Second, the effect of the pulse fluence is investigated in terms of the topology and morphology of the pellets. Here, the arithmetic surface roughness Ra is the main parameter. Then, the depth of the radiation interaction in the pellet is measured. The focus of this paper is on the different pulse widths of the laser sources, and therefore, similar pulse and hatch overlap ensure equivalent areal energy input in both cases. As a summarized result, treatment with a shorter pulse width generates high peak pulse powers, resulting in higher temperatures, rougher surfaces and affecting deeper layers of the pellets compared to treatment with longer pulse width. On the contrary, excessive power leads to the ablation of the material up to destruction.

Keywords Laser sintering · Laser-material interaction · Ceramic ion conductor · LATP · All-solid-state batteries

1 Introduction

All-solid-state batteries (ASSB) are considered the next-generation batteries due to benefits in safety, gravimetric and volumetric energy density and temperature operating window compared to established liquid electrolyte-based batteries [1, 2]. However, concepts with latent qualities, which may be developed and lead to future success, contain a lithium metal anode, a composite cathode and an inorganic separator [3]. The last-mentioned component is non-flammable, leading to an intrinsically safe full ceramic solid-state battery with outstanding mechanical properties. The synthesis and processing of the ceramic solid electrolyte play a major role in the realization of this cell concept and currently different types are being investigated, such as the garnet-type $Li_7La_3Zr_2O_{12}$ (LLZO) [4] and the NASCION-type $Li_{1+x}Al_xTi_{2-x}(PO_4)_3$ (LATP) [5, 6]. In particular, the LATP has excellent properties in terms of cost-effective production, processing and satisfactory ionic conductivity. The reduction of Ti^{4+} to Ti^{3+} in contact with lithium metal is considered the greatest weakness. To circumvent this circumstance, researchers are attempting to stabilize the boundary interfaces, e. g. with sandwich structure with $Li_{1+x}Al_xGe_{2-x}(PO_4)_3$ (LAGP) [5, 7]. Regarding different solid electrolytes, such as LATP, studies mainly focus on the properties of the material.

However, a densification process is required to obtain the mobility of Li^+ in the solid electrolyte and lower the grain boundary resistance of the LATP. Usually, furnace sintering processes are applied but non-flexible process integration combined with a long-lasting sintering period limits their usage [8]. In addition to the conventional heat treatment, several rapid sintering processes as field-assisted sintering technologies (FAST) are being investigated to reduce process time [9]. Although processing with these methods significantly reduces the processing time, some research reports detrimental material properties, such as lithium loss or structural defects [10]. Furthermore, the systems possess disadvantages, for instance, in the flexibility of the sample geometry. Both sintering methods are not suitable for large-scale production and limit the quick success of ASSB with ceramic ion conductors.

✉ H. Wehbe
h.wehbe@tu-braunschweig.de

[1] Institute of Joining and Welding, Technische Universität Braunschweig, Langer Kamp 8, 38106 Brunswick, Germany

To establish the ceramic materials in the solid-state battery, it is necessary to develop competitive methods in material synthesis and sintering. Since the sintering also affects the material properties of the final product, it is important to extend the knowledge on the interconnection between both. Concerning the processing, the long-term aim is to manufacture economically in a large-scale industrial environment.

In the fields of science, industry and medicine, coherent and monochromatic irradiation of high intensity has found various applications. Moreover, lasers are also established in the production of battery cells [11] and are mostly used for welding the housing [12] and electrodes [13], for separating [14] and structuring electrodes to improve their functionality [15]. The usage of future battery materials, e. g. lithium metal anodes [16, 17], is also desired to justify the high acquisitions costs. In addition, the interaction with materials is a complicated phenomenon [18–21] and has been a subject of countless investigations. So, the need for research is still high to understand the insufficiently known phenomena.

In the present study, the usage of electro-magnetic laser irradiation as a new sintering process for LATP is under investigation. Especially, two laser systems with different pulse widths are compared under variation of the irradiance. The sintering behaviour of both systems is analysed by a simultaneous temperature measurement, recorded by an infrared camera and the achieved properties of the samples in terms of their surface topology characterized by a laser scanning microscope and the interaction depth of the irradiation determined by a scanning electron microscope. The aim is to evaluate the sintering ability using lasers and to determine the effect of the pulse width.

2 Experimental setup

The LATP powder is provided by Schott AG with an average diameter of $d_{50} = 1{,}2$ µm. To determine the sintering ability through electro-magnetic laser irradiation, 300 mg of the provided LATP powder is first filled into a die and then pre-compressed to pellets using a uniaxial hand press. The compacting force is set to 78 kN and held for 30 s. A force limiter and a timer ensure that both force and time are maintained. On average, this procedure results in pellets with a diameter of 16 mm and a height of 80 µm.

In this work, two laser sources with a wavelength in the range of 1062 ± 3 nm are used for processing in pulse mode. The main difference between the sources is that Laser A has a pulse width of 250 ns and Laser B has a pulse width of 8.6 ps. Table 1 shows the comparison of the adjustable characteristics of both sources. The average output power P_{AVG} is selected from minimum to maximum in steps of 5 W for both systems to adjust the fluence (energy per area in consideration of the pulse repetition frequency). The connection between these parameters is shown in Fig. 1.

In addition to the laser properties, the processing strategy and thus the areal energy input in the LATP pellet is important. To guarantee identical processing conditions, some framework conditions are the same as the pulse repetition frequency f of 100 kHz. Due to the different spot diameters d_{Spot}, the scanning velocity v is adjusted for each system individually. This is one way to ensure similar energy input per area. Conventionally, the so-called pulse overlap (PO) is used for this purpose, which harmonizes the parameters pulse repetition frequency f, scanning velocity ν and spot diameter d_{Spot}. Figure 1 illustrates this intention and gives the formulaic relationship.

Three overlap values (PO 50%/ PO 75%/ PO 95%) are used for the investigation in this work and the resulting velocities are given in Table 2. In addition, a hatch overlap (also known as line spacing) of 50% is set for both sources.

To characterize the correlation between the irradiation and material behaviour in dependency on the pulse width, four major measurements were performed in total. During the entire laser heat treatment, the surface temperature (I, Fig. 2) of the pellets is measured with an infrared camera (VarioCAM HD head, Infratec). The framerate is 120 Hz and possible image sizes are up to 1024×96 pixels. Here, the centre of interest is the averaged maximum temperature in the middle section of the pellet, which is only in the ranges from 20 to 75 pixels. In this study one pixel of the infrared camera corresponds to 0.178 mm of the real pellet.

Subsequently, optical evaluations were used to determine the influence of the irradiation on the LATP pellets. For this purpose, the surfaces are individually recorded using a digital light microscope (VHX 2000, Keyence) to document any changes (II). Afterwards, the surface roughness (III) was determined with a laser scanning microscope (LSM) (VK-9710 3D, Keyence). For this purpose, the arithmetic surface roughness Ra is determined for each pellet at five surface

Table 1 Properties of used laser systems

Property	Laser A	Laser B
Product	SPI redENERGY G4	Coherent Hyper Rapid 50-F
Wavelength *nm*	1062 ± 3 nm	
Average Output Power *W*	70	60
Pulse Width *ns*	250	0.086
Pulse Repetition Frequency *kHz*	55 - 500	100 - 500
Spot Diameter *mm*	0.08	0.044
Operating mode	Pulsed	

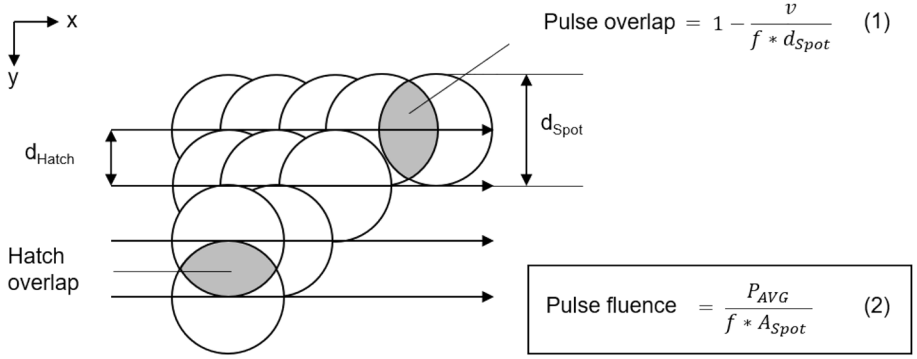

Fig. 1 Relationship between single laser spot and areal irradiation including pulse fluence

Table 2 Corresponding scanning velocities

Source	PO 50%	PO 75%	PO 95%
Laser A	4000 mms^{-1}	2000 mms^{-1}	400 mms^{-1}
Laser B	2200 mms^{-1}	1100 mms^{-1}	220 mms^{-1}

positions. In the last step, the samples are broken in the middle and the fracture edge is observed with a scanning electron microscope (SEM) (Phenom XL, Thermo Fischer Scientific Inc.) to measure the interaction depth (IV). Figure 2 shows a schematic representation of the measurement methods.

To evaluate the process, the crystallographic structure of the laser sintered pellets was identified by X-ray diffractometry (Empyrean range, Malvern Panalytical) and CuKα radiation at 40 kV and 40 mA. The angle range is between 15° and 40° with 0.05° steps. With this method, secondary phases can be detected and used to evaluate the laser process.

3 Results and discussion

3.1 Real-time temperature monitoring

In the following, the temperatures of the LATP pellets for different pulse fluences are shown as a function of the three pulse overlaps processed with Laser A. In general, Fig. 3 shows an increase in output power and thus in pulse energy, which leads to an increase in surface temperature. This progression is nearly linear for all test series, but the slopes are different.

For a pulse overlap of 50%, the temperature reaches a maximum of 117 °C at 14 Jcm^{-2}. An elevation to 75% leads to an analogous curve, but at higher temperatures. The maximum temperature is 220 °C. In comparison to a PO of 95%, the surface temperature increases significantly from 5 Jcm^{-2} than for the other two POs. This circumstance can be explained by the fact that with higher overlap more pulses impinge on the similar area increment (Fig. 1), and thus, the energy input per area rises. As a result, the pulse energy heats the pellets' surface.

The curves for Laser B can be observed in the graph in Fig. 3b. The temperature curves for PO 50% and 75% are almost identical and reach a maximum of 324 °C and 360 °C, respectively. For the PO 95%, the temperature rises abruptly from 13 Jcm^{-2} and surpasses the maximum temperature of the other two curves here. Furthermore, it can be observed that a maximum is reached for all POs from 23 Jcm^{-2} onwards. Here, an increase in average output power no longer leads to an increase in temperature. For the PO 95%, the temperature is 1350 °C. This value corresponds to the maximum recordable of the infrared camera. Ristic et al. [20] document similar behaviour in

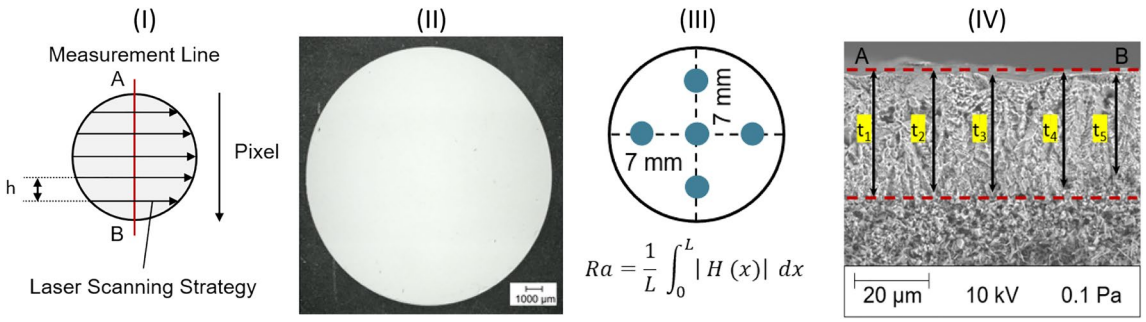

Fig. 2 Measurement routine

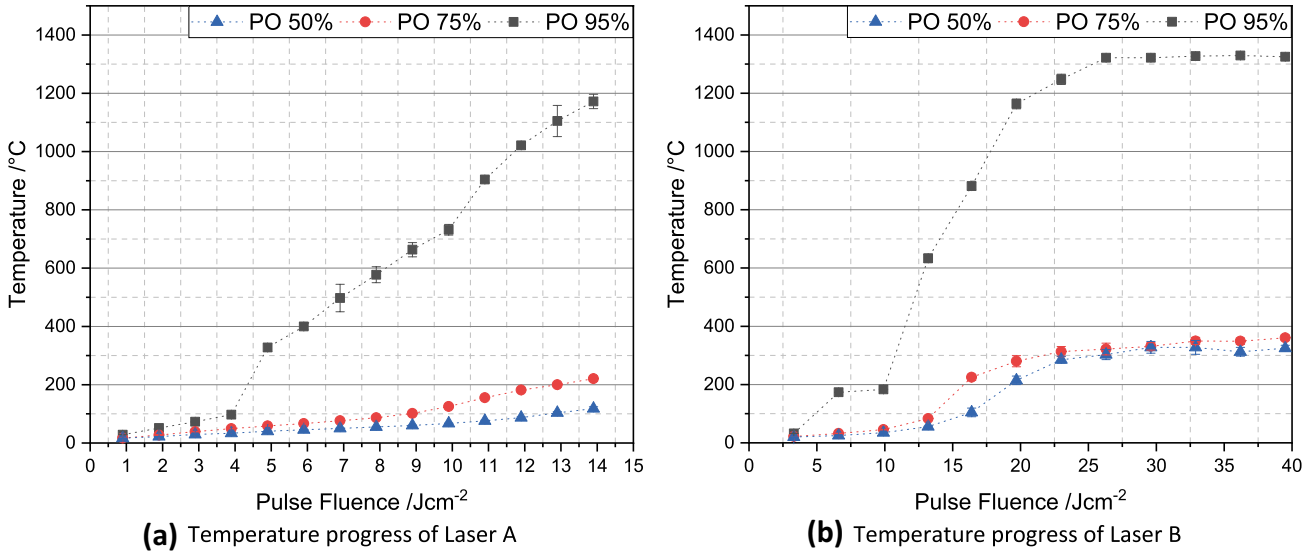

Fig. 3 Temperature progression during real-time treatment in dependency on the pulse width

their work, while processing a ceramic tile with a Nd:YAG laser.

If both laser sources are compared, the temperatures of Laser B are always higher than those of Laser A. This is since the pulse peak power P_{Peak}, which takes the pulse width τ into account, is significantly higher for Laser B than for Laser A. For instance, a P_{AVG} of 60 W (pulse fluence 40 Jcm^{-2}) at Laser B delivers a pulse peak power of 69.8 MW compared to 2.8 kW at 70 W (pulse fluence 14 Jcm^{-2}) for Laser A.

$$P_{Peak} = \frac{P_{Avg}}{f * \tau}. \quad (2)$$

3.2 Surface topologies and roughness

This section shows the surfaces after laser processing. Table 3 shows exemplary structures from the microscope and SEM micrographs prepared with the three pulse overlaps at the highest power (14 Jcm^{-2}) for Laser A.

From the microscope images, no change in the surface of the PO 50 % can be observed in comparison with the pressed pellets (Fig. 2, II). At a higher macroscopic magnification in the SEM first changes in the surface can be detected, but these changes only occur in specific areas. Pulse fluences below 7 Jcm^{-2} do not lead to any changes in the material's surface.

Table 3 Surface structure for processing with Laser A at 14 Jcm^{-2} pulse fluence

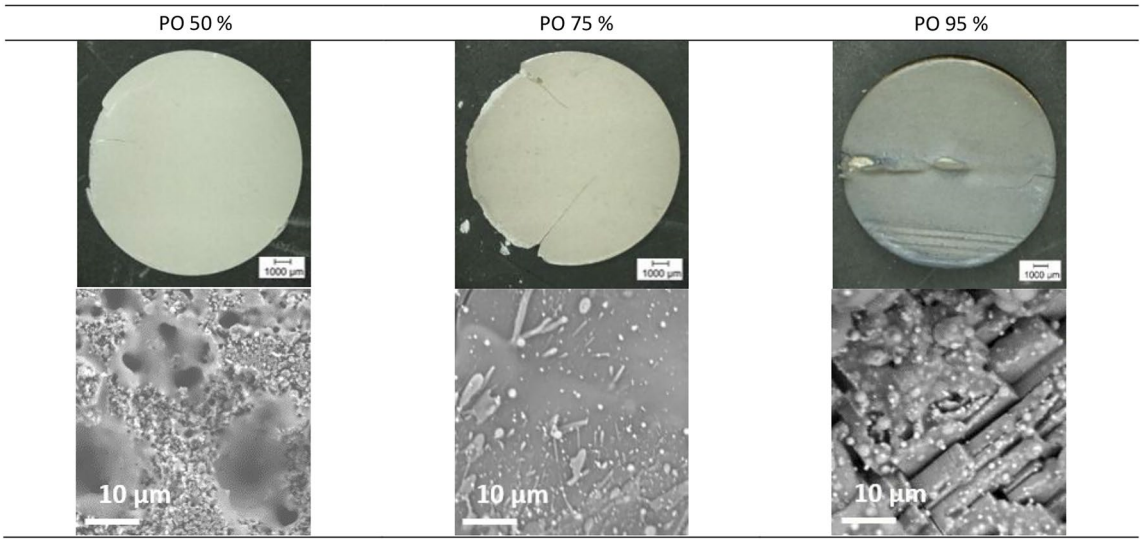

At PO 75%, the surface transforms into a yellow–brown colour and the SEM image shows a solidified melt, which is additionally supplemented by spheres and stripes. This interaction is only documented from a pulse fluences of 12 Jcm^{-2} and the tendency to melt increases with increasing power. In [20], this effect is described as an undesirable effect of melting and rapid re-solidification of the amorphous component. On the opposite, Mühler et al. [22] refers to a solidified molten mass. In both cases, however, other ceramics are used as a substrate and not LATP. The spotty treatment as in PO 50% is observed at pulse fluences between 9 Jcm^{-2} and 11 Jcm^{-2}.

At PO 95%, the pellet has a grey colouration after processing and a chequered pattern can be observed in the SEM image, complemented by spherical ejections in the micrometre range. Due to the energy input, the pellet bulges in the centre, so that the edges remove themselves from the processing substrate.

Table 4 shows the same overlaps for the processing with the Laser B. PO 50% and PO 75% show similar brownish surfaces but in contrast at PO 95% the pellet is grey. Furthermore, the pellet is almost destructed entirely, which indicates that the energy input leads to ablation and evaporation of the material. [23, 24]

Due to the higher energy input than with the nanosecond laser, the pellets with the PO 50% already have the surface structure at PO 75% from Laser A. However, more ejections can be observed here. An increase in the pulse overlap leads to a higher number of spheres on the surface.

Already at this point, some conclusions can be drawn, such as how a variation of the pulse width affects the sintering of LATP pellets. High energy input, as in the case of the Laser B with PO 95%, is not acceptable from 20 Jcm^{-2} onwards, since the irradiation begins to gradually dissipate the pellet and thus destroy it at the end of the processing. In the literature [20] this effect is referred to as the spallation mechanism.

The surface roughness is determined by the LSM at five points on the pellet and Fig. 4 displays the values for both lasers. The untreated pellets are considered as a reference and have a Ra value of 4.60 ± 0.64 µm.

For processing with nanosecond pulses (Fig. 4a) Ra is always within the standard deviation of the reference for a pulse overlap of 50% and confirms the optical impressions, since no change in the surfaces is visible in the SEM. With an increase to PO of 75%, the pellets show a comparable behaviour up to 10 Jcm^{-2}. Beyond 33 Jcm^{-2}, the arithmetic surface roughness Ra is higher than the reference. The limit shifts down towards 5 Jcm^{-2} for PO 95% and an increase in pulse fluence leads to higher roughness.

In comparison, processing with picoseconds (Fig. 4b) has a different effect on the surface roughness. Up to 10 Jcm^{-2} Ra is almost constant for all parameters and in the range of the reference pellet. With an overlap of 50%, the roughness is on average always below 10 µm, whereas PO 75% and 95% showed significantly higher roughness than the untreated pellets. The difference between these two overlaps is marginal and only deviates for 20 Jcm^{-2}. This equality indicates that the energy input may differ in terms of temperature, but the resulting surfaces are different.

Additionally, the interactions lead to stochastically distributed spherical ejections on the surface with a diameter of approx. 5 µm. These lead to an increase in the roughness of the surface, which is also reinforced by grooves and cracks. The larger standard deviations can be traced back to the removal of the material, which is visible in the laser process and through the shape deviation, which is represented by the

Table 4 Surface structure for processing with Laser B at 40 Jcm^{-2} pulse fluence

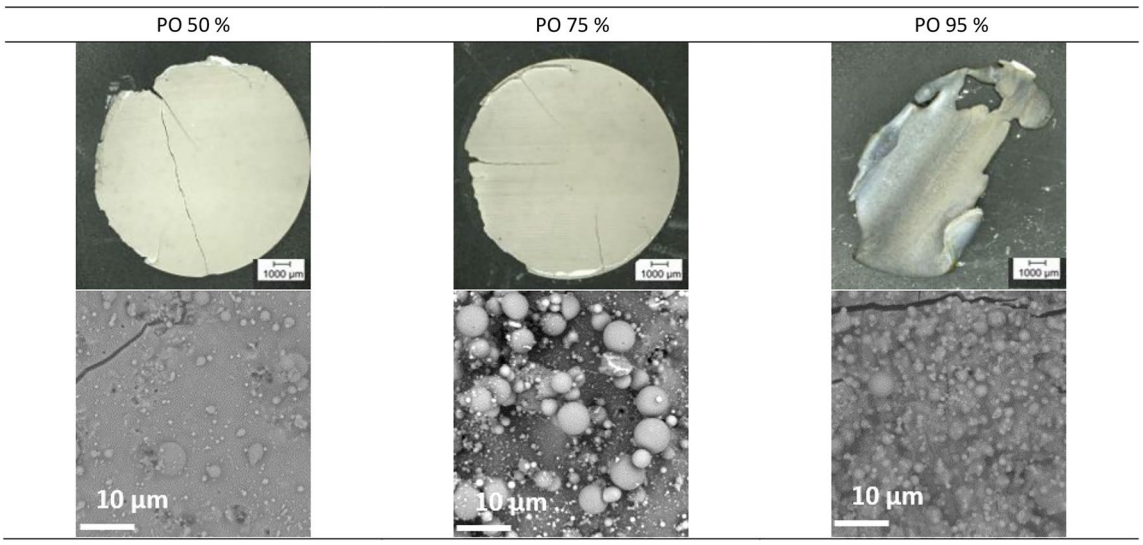

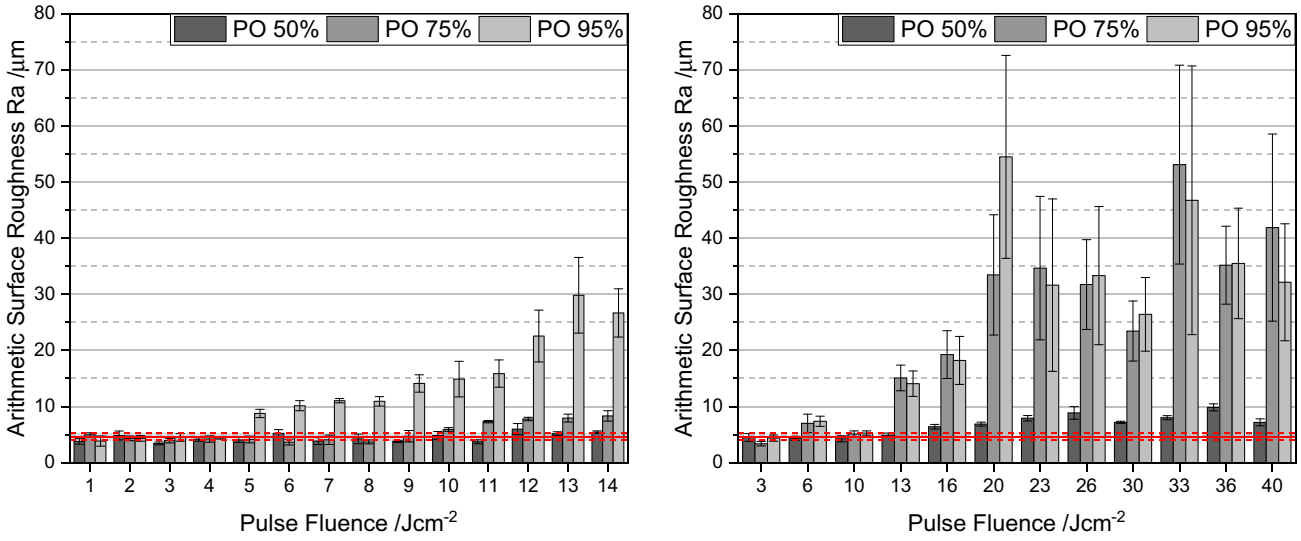

(a) Arithmetic surface roughness of pellets processed with Laser A

(b) Arithmetic surface roughness of pellets processed with Laser B

Fig. 4 Comparison of the arithmetic surface roughness

waviness. These circumstances also lead to higher Ra values when using Laser B than with Laser A.

The change in surface roughness due to the processing of zirconia ceramics using laser irradiation (Nd:YAG and CO_2) is also documented in Namdar et al [25]. Their work aims to remove material without temperature impact. Even if the roughness could be increased, the authors declared these lasers as not suitable for ceramic because the irradiation causes an increase in temperature through absorption, which changes the material properties. One of these changes is the formation of a melt and an amorphous phase, as well as microcracks [20]. In contrast, this heat treatment is necessary for sintering. Microcracks and foreign phases shown in [26] are not desired in the sintering of LATP and lower the ionic conductivity. The influence of these must be addressed in further work, to evaluate the laser sintering for LATP.

3.3 Interaction depth

The sintering behaviour in terms of interaction depth was investigated with a SEM. For this purpose, the pellets were broken in the middle and the fracture edge is irradiated with an electron beam. The interaction depth is declared from the upper edge to the depth to which the laser irradiation still causes a change in the pellet. Figure 5 shows the results as a function of the pulse fluence and the pulse overlaps for both laser sources.

The following behaviour is shown for processing with Laser A: In total, the energy input at PO 50% is not sufficient to initiate the sintering process. In the fracture edge of the pellets, no interaction can be observed. At PO 75%, no interaction can be observed up to 7 Jcm^{-2}. Scattered selective changes in depth are observed from 8 Jcm^{-2} to 11 Jcm^{-2}. From 12 Jcm^{-2}, united layers emerge, which have a thickness of about 3 µm.

Increasing the energy per area to PO 95% provides higher layer thicknesses. With pulse fluence up to 4 Jcm^{-2}, the energy of the pulses is deficient to cause a permanent interaction and between 5 Jcm^{-2} and 8 Jcm^{-2}, an almost constant depth is achieved. From 9 Jcm^{-2}, the interaction depth increases proportionally with increasing power.

Taking the previous results from the temperature and the roughness into account, the results of the interaction depth confirm the impression that with higher geometrical energy input the effects on the pellets become more obvious. For PO 50% and PO 75%, the energy input is not significant to cause a change in the pellet and only with a high energy input the material change can be initiated.

In comparison to the processing with the picosecond laser, the interaction depth behaves equivalently. The intensity which must be exceeded for a sintering reaction is lowered in the direction of lower pulse influences. At higher powers, greater depths can be realized, but the pellets' integrity cannot be maintained due to the ablation. Therefore, only the remains of the pellets are used to determine the interaction depth at PO 95 %. Nevertheless, an interaction depth corresponding to the total thickness of the pellets could be measured here.

Bucharsky et al. [27] describes the thermal conductivity λ of LATP as a function of the sintering temperature and reveals that higher sintering temperatures lead to higher thermal conductivities (0.7 Wm^{-1} K^{-1} and 2 Wm^{-1} K^{-1})

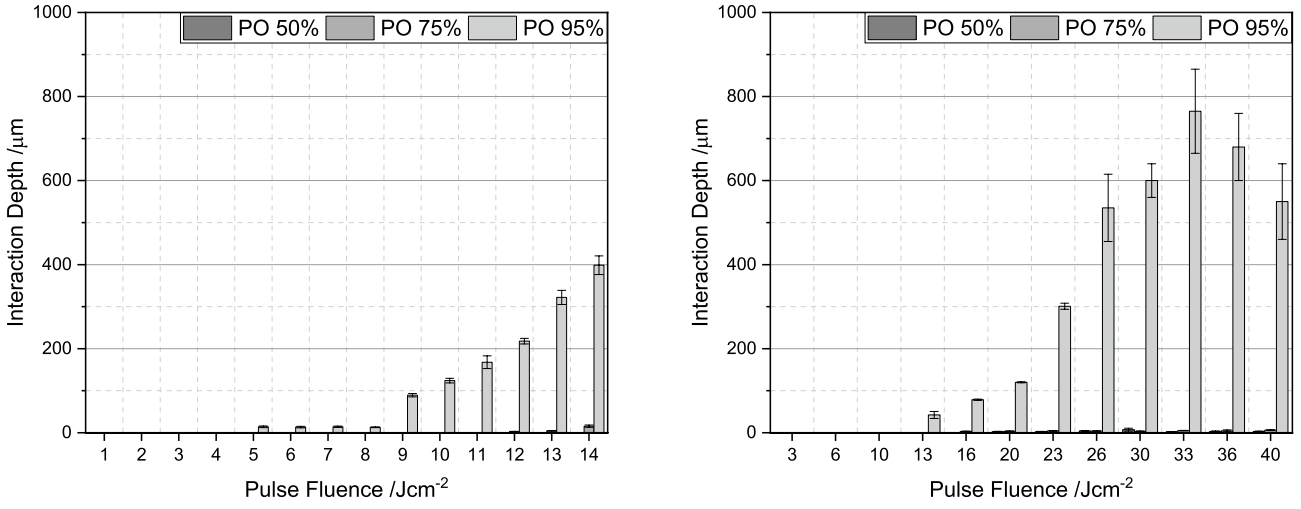

Fig. 5 Comparison of the interaction depth

and simultaneously a reduction in porosity. The investigation range applies to sintering temperatures between 800 °C and 1000 °C. [27] A transfer to the presented outcomes shows that elevated interaction depths are achieved with an increase in the sintering intensity by increasing the energy input.

3.4 X-ray diffraction

Based on these findings, the most promising results from processing with Laser A (nanosecond) were further characterized to verify the crystallographic structure. The XRD measurements were carried out for a non-sintered but compressed pellet (REF) and two pellets from the PO 95% processing and different pulse fluence (6 Jcm^{-2} and 13 Jcm^{-2}). Figure 6 shows the results.

The main peaks in the diffractogram are at similar positions compared to the reference. This circumstance indicates no fundamental change in structure. [27, 28] Regarding the peak intensity, a higher pulse fluence leads to changes in intensity. Various scientific papers refer to this phenomenon as a dependency on temperature. Elevated temperature leads to higher intensities. [8, 27, 29, 30] Similarly, the intensity decreases for the peak at 24.7° (13 Jcm^{-2}) and indicates a change in the amount of the crystal´s orientation. A possible explanation is that the proportions of different layers overlap [22]. However, and more importantly, the presence of secondary phases, such as $AlPO_4$, which is typically proven with a peak around 21.5°, cannot be observed here. In the literature, the formation of this phase occurs at sustained high temperatures and decreases the ionic conductivity due to the blocking of ionic pathways in the LATP framework. [8, 27, 31] In addition, TiO_2 usually arises alongside with

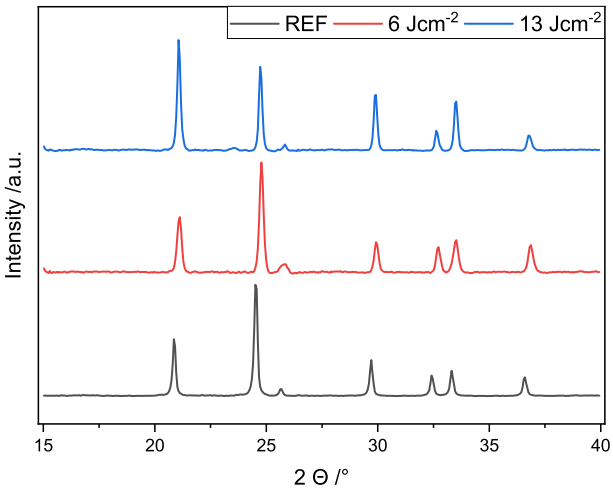

Fig. 6 XRD pattern for compressed (REF) and two LATP pellets prepared with Laser A

$AlPO_4$. This impurity phase usually demonstrates lithium loss and can be observed with a peak around 25° next to the shown peak. [31] Since the locally prevailed maximum temperature only acts for a short period, the irradiation is not sufficient to initiate this reaction.

4 Conclusion

In general, the comparison of different laser sources is challenging due to the dissimilar characteristics of the systems. Therefore, two lasers from the infrared range were selected and similar pulse overlaps are used to create an

identical geometric energy input. Thus, the difference between both sources on the sintering of LATP can only be determined concerning the pulse width. Temperatures, surfaces, roughness and depth of interaction are used to evaluate sintering suitability and the effect of the pulse width.

As a result, a single pulse is not sufficient to achieve an interaction for all evaluation criteria. Only by increasing the energy per surface with the pulse overlap the number of hits per increment leads to an interaction with the material. However, the role of the pulse duration is of little importance in the case of small overlaps. In the case of the highest overlap, it takes on a decisive role and leads to a higher surface temperature and enables volume sintering. Nevertheless, it must be considered that energy input can not only be used for sintering but also for material ablation up to the destruction of the pellet. The comparison of the pulse peak power shows that Laser A is in the kW range, whereas Laser B is in the MW range and thus higher by a factor of 1000.

In conclusion, the investigations in this work show the ability of sintering LATP using electro-magnetic irradiation due to the absorption of the radiation energy by the pellets. In the used configuration, however, the processing is challenging because the irradiance, especially with the short pulse width, is not only used for sintering but also for material ablation. This ablation is not the intention and so further investigations with adjusted parameters are necessary, for instance, a pulse overlap between 75 and 95%.

Promising results from the experiments with the Laser A were further investigated using XRD. Secondary phases that limit the ionic conductivity were not found. This shows that the sintering of LATP is possible with a suitable choice of parameters and pulse width as in Laser A. In summary, this work demonstrates the applicability of laser irradiation for sintering of LATP.

Moreover, the advantage of full flexibility in laser processing is not enabled in this procedure. To fully develop the potential of laser processing, a layer-by-layer deposition and sintering while the bulk of the material is unaffected (according to the models in 3D printing) can be the subject of the next investigations, as well as the investigation of the crystal structure and ionic conductivity after sintering in regard to the implementation in the battery. Properties in terms of changes in chemical composition or decomposition and porosity should also be part of further discussions.

Acknowledgements The authors acknowledge the Federal Ministry of Education and Research and Projektträger Jülich for their support in the project 3D-SSB (funding code 03XP0202F). There is no conflict of interest.

Funding Open Access funding enabled and organized by Projekt DEAL.

Declarations

Conflict of interest Not applicable.

References

1. H. Aono, E. Sugimoto, Y. Sadaoka, N. Imanaka, G. Adachi, J. Electrochem. Soc. **136**, 590 (1989)
2. F. Zheng, M. Kotobuki, S. Song, M.O. Lai, L. Lu, J. Power Sources **389**, 198 (2018)
3. K.J. Kim, M. Balaish, M. Wadaguchi, L. Kong, J.L.M. Rupp, Adv. Energy Mater. **11**, 2002689 (2021)
4. P. Barai, T. Fister, Y. Liang, J. Libera, M. Wolfman, X. Wang, J. Garcia, H. Iddir, V. Srinivasan, Chem. Mater. **33**, 4337 (2021)
5. R. DeWees, H. Wang, Chemsuschem **12**, 3713 (2019)
6. G. Yan, *Mechanical behavior of solid electrolyte materials for lithium-ion batteries* (RWTH Aachen University, 2020)
7. E. Zhao, F. Ma, Y. Guo, Y. Jin, RSC Adv. **6**, 92579 (2016)
8. K. Waetzig, A. Rost, C. Heubner, M. Coeler, K. Nikolowski, M. Wolter, J. Schilm, J. Alloy. Compd. **818**, 153237 (2020)
9. Y. Liu, J. Liu, Q. Sun, D. Wang, K.R. Adair, J. Liang, C. Zhang, L. Zhang, S. Lu, H. Huang, X. Song, X. Sun, ACS Appl. Mater. Interfaces **11**, 27890 (2019)
10 N. Hamao, Y. Yamaguchi, K. Hamamoto, Materials (Basel, Switzerland) **14**, 4737 (2021)
11. W. Pfleging, Nanophotonics **7**, 549 (2018)
12. S. Hollatz, S. Kremer, C. Ünlübayir, D.U. Sauer, A. Olowinsky, A. Gillner, Batteries **6**, 24 (2020)
13. S. Grabmann, J. Kriegler, F. Harst, F.J. Günter, M.F. Zaeh, Int. J. Adv. Manuf. Technol. **118**, 2571 (2022)
14. T. Jansen, M.W. Kandula, D. Blass, S. Hartwig, W. Haselrieder, K. Dilger, Energy Technol. **8**, 1900519 (2020)
15. J.B. Habedank, J. Endres, P. Schmitz, M.F. Zaeh, H.P. Huber, J. Laser Appl. **30**, 32205 (2018)
16. L. Schmidt, H. Wehbe, M.W. Kandula, K. Dilger, in Tagungsband 4. Symposium Materialtechnik (Shaker Verlag Düren, 2021), p. 521
17. T. Jansen, S. Hartwig, D. Blass, K. Dilger, *International congress on applications of lasers and electro-optics* (Laser Institute of America, 2017), p.602
18 J. Dutta Majumdar, I. Manna, Sadhana **28**, 495 (2003)
19 C. Webb, J.D. Jones, *Handbook of laser technology and applications* (CRC Press, 2020)
20. S. Ristic, S. Polic, B. Radojkovic, J. Striber, PAC **8**, 15 (2014)
21. D. Knezevic, B. Radojkovic, S. Ristic, S. Polic, M. Janicijevic, L. Tomic, B. Jegdic, Therm. Sci. **25**, 567 (2021)
22. T. Mühler, Laser-Materie-Wechselwirkung beim Selektiven Laser Sintern von Keramik (Technischen Universität Clausthal, 2017)
23. D. Sola, A. Escartín, R. Cases, J.I. Peña, Appl. Surf. Sci. **257**, 5413 (2011)

24 X. Jia, Y. Chen, L. Liu, C. Wang, J. Duan, Nanomaterials (Basel Switzerland) **12**, 230 (2022)
25. S.F. Namdar, N. Chiniforush, M.H. Tabatabae, Arami Sakineh. J. Dent. **11**, 233 (2014)
26. B. Davaasuren, F. Tietz, Solid State Ionics **338**, 144 (2019)
27. E.C. Bucharsky, K.G. Schell, T. Hupfer, M.J. Hoffmann, M. Rohde, H.J. Seifert, Ionics **22**, 1043 (2016)
28. S. Soman, Y. Iwai, J. Kawamura, A. Kulkarni, J. Solid State Electrochem. **16**, 1761 (2012)
29. T. Hupfer, Herstellung von LATP für den Einsatz als Festkörperelektrolyt und dessen Eigenschaften (2017)
30. Y. Lin, N. Luo, E. Quattrocchi, F. Ciucci, J. Wu, M. Kermani, J. Dong, C. Hu, S. Grasso, Ceram. Int. **47**, 21982 (2021)
31. M.I. Kimpa, M.Z.H. Mayzan, F. Esa, J.A. Yabagi, M.M. Nmaya, M.A. Agam, J. Sci. Technol. **9**, 106 (2017)